Geotechnical Aspects of Underground Construction in Soft Ground – Viggiani (ed)
© 2012 Taylor & Francis Group, London, ISBN 978-0-415-68367-8

3D finite element analysis of deep excavations with cross-walls

S. Rampello & S. Salvatori
"Sapienza", University of Rome, Italy

ABSTRACT: Ground movements induced by deep open excavations retained by diaphragm walls may be substantially reduced using sacrificial cross-walls installed as props between the retaining walls. In this paper, a 3D finite element study is presented in which the retaining walls and the cross-walls are modelled using brick elements and accounting for the interfaces between the panels of diaphragm walls and of cross-walls. Influence of cross-walls spacing and length in reducing the horizontal deflection of diaphragm walls and the ground settlements behind the excavation is evaluated. Companion plane strain analyses, in which an homogeneous equivalent medium is considered in between the retaining walls, are also presented to assess the capability of 2D analyses to predict the performance of deep excavations in which cross-walls are used as a mitigation measure to reduce wall deflections and ground movements.

1 INTRODUCTION

Constructions of deep box excavation in soft ground generally result in ground movements that can induce significant damage to adjacent buildings and services. To reduce their impact, box excavations are usually retained by stiff diaphragm walls and props installed as the excavation progresses. However, vertical stress relief associated to excavation induces surface settlements even when the retaining walls are prevented from moving horizontally and deep-seated inward displacements of the walls that cannot be controlled by the props that are installed within the excavation itself (Burland et al., 1979).

To minimise the impact of deep excavations in urban areas, inward displacements of diaphragm walls and surface settlements around excavations may be reduced installing an internal support system below the formation level, prior to excavation. Such a system of deep in situ props may be constituted by tunnelled struts (Stevens et al., 1977; Bailey et al., 1999), ground treatment methods such as jet mechanical mixing (Osborne et al., 2009) and jet grouting, used to replace the soil below the final excavation level, or sacrificial cross-walls (Hsiung et al., 2001; Ou et al., 2006; Hsieh et al., 2008). Cross-walls can be formed by jet grouted columns or unreinforced panels installed with diaphragm walling equipment. They are installed between the perimeter diaphragm walls before the start of excavation and are excavated out with the soil down to the depth of the final excavation level. At the end of the excavation sequence, the only portion of the cross-walls remaining to resist to the horizontal deflection of the diaphragm walls is that eventually extending below the bottom of excavation.

In recent years, cross-walls have been often used in deep excavations in urban Taiwan area to reduce diaphragm wall deflections and associated ground movements. Well documented case histories permitted to assess the effectiveness of cross-walls in reducing excavation-induced displacements (Hsiung et al., 2001; Ou et al., 2006), provided that the joints between the perimeter diaphragm walls and the cross-walls are well constructed (Hsieh et al., 2008). The beneficial effects were evaluated by comparing horizontal wall deflections monitored at locations affected by the presence of cross-walls with those measured at sites with no special support (Hsiung et al., 2001) or computed under plane strain conditions assuming no cross-walls (Ou et al., 2011).

Effectiveness of cross-walls in reducing wall deflections and ground movements has been recently studied by Merrit et al. (2010) via 3D finite element analyses in which the retaining walls and the props were represented by shell elements and the cross-walls by membrane elements; specifically, influence of horizontal axial stiffness of cross-walls relative to that of perimeter retaining walls was assessed.

This paper deals with a 3D finite element study of deep excavations in which the diaphragm walls and the cross-walls are modelled using brick elements and the contacts between the corresponding panels are represented by interface elements.

Excavations were modelled without cross-walls and with cross-walls of different length, installed at different spacing. To assess the capability of 2D analyses to predict the performance of deep excavations with sacrificial cross-walls, plane strain analyses were also carried out in which an equivalent material is used to represent the soil and the cross-walls within the excavation.

2 PROBLEM DESCRIPTION

2.1 *Soil profile and constitutive model*

Ground conditions adopted in the analyses are representative of those encountered in the historical centre of Rome, close to the Tiber river. The soil profile shown in Figure 1 consists of medium dense gravelly Made Ground, with an average thickness of 9 m, overlying recent alluvial deposits of Pleistocene age. They consist of slightly overconsolidated clayey silt, about 6 m in thickness, medium dense silty sand, 15 m thick, normally consolidated silty clay, 27 m in thickness and sandy gravel, of 6 to 8 m thick. The gravel is underlain by a thick layer of stiff and overconsolidated silty clay of Pliocene age.

Figure 1 show typical profiles of tip resistance q_c measured by CPTU tests and of small-strain shear modulus G_0 as obtained by Cross Hole tests. The profile of pore water pressure was observed to be hydrostatic with hydraulic head at about the bottom of the Made Ground.

The mechanical behaviour of all soils was described using an elastic-plastic rate independent model with isotropic hardening (*Hardening Soil*, *HS*; Schanz et al. 1999), available in the model library of the code Plaxis. The model is capable of reproducing soil non-linearity due to the occurrence of plastic strains from the beginning of the loading process.

The elastic behaviour is defined by isotropic elasticity through a stress-dependent Young's modulus:

$$E' = E^{\text{ref}} \left(\frac{c' \cdot \cot \varphi' + \sigma_3'}{c' \cdot \cot \varphi' + p^{\text{ref}}} \right)^{\text{m}} \quad (1)$$

where σ'_3 is the minimum principal effective stress, c' is the cohesion, φ' is the angle of shearing resistance and p^{ref} = 100 kPa is a reference pressure; E^{ref} and m are model parameters.

The model has two yield surfaces, f_s and f_v, with independent isotropic hardening depending on deviatoric plastic strain γ^p and on volumetric plastic strain ε^p_v, respectively. The deviatoric hardening rule is related to parameter E'_{50}, while the volumetric one is controlled by parameter E'_{oed}. Both of them are given by expressions similar to Eq. (1) but, in contrast to E', they are not used within a concept of elasticity. The flow rule is associated for states lying on the surface f_v, while a non-associated flow rule is used for states on the surface f_s.

Under monotonic loading, *HS* model can account for non-linear stress–strain behaviour, with tangent initial modulus equal to E', and for the occurrence of irreversible strains from the beginning of the loading process. Upon unloading, the model assumes elastic behaviour with Young's modulus E', thus reproducing a significant change in stiffness.

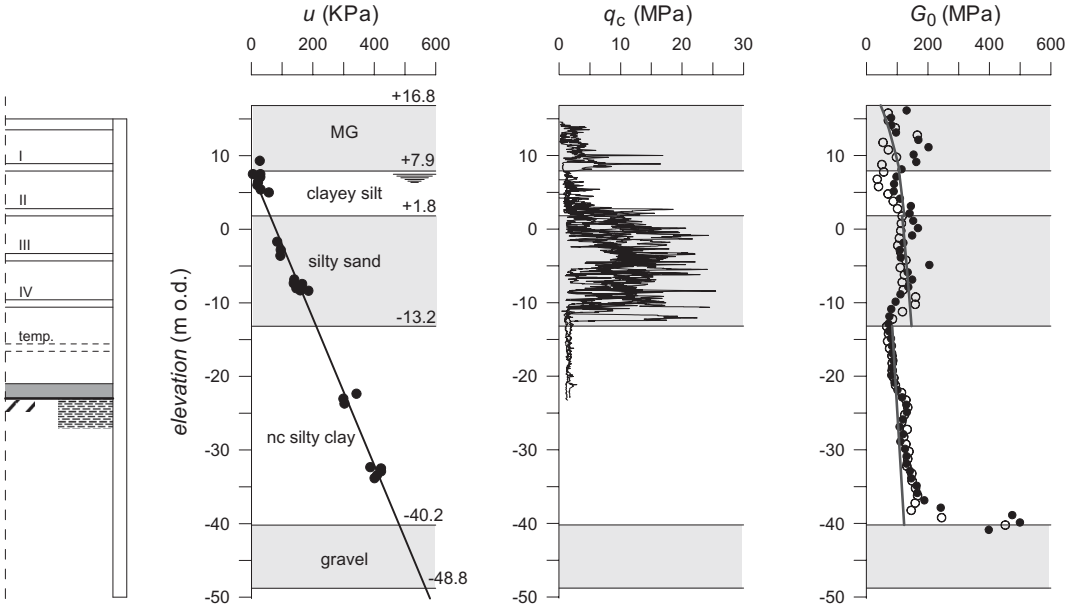

Figure 1. Vertical section of the excavation with soil profile.

Since E' represents the tangent initial Young's modulus of the stress-strain curve, it has been related to the shear modulus at small strains G_0 obtained from Cross Hole tests. In particular, values of E^{ref} and m were obtained by best fitting the cross-hole test results using Eq. (1) and assuming $\nu' = 0.2$. The continuous line in Figure 1 represents the prediction of G_0 obtained with the values of c', φ', E^{ref} and m reported in Table 1. Specifically, the values of σ'_3 needed for computing E' were obtained using the values of the coefficient of earth pressure at rest K_0 listed in the table.

It is worth mentioning that OCR has to be regarded as a Yield Stress Ratio (YSR) defined in the framework of strain hardening plasticity, so that values of $OCR > 1$ can be specified also for geologically normally consolidated soil layers exhibiting a yield stress larger than the in situ stress; this was the case for the granular soils such as the made ground and the layers of sand and gravel.

Stiffness decay with shear strain was described using ratios of $E^{ref}/E^{ref}_{50} = 15$ for the normally consolidated silty clay, 20 for the stiff over-consolidated clay deposit and 10 for the remaining soil layers; $E^{ref}_{50}/E^{ref}_{oed} = 1$ and an angle of dilatancy at failure $\psi = 0$ were adopted for all soils; these values provided a satisfactory fitting with the stress-strain curves observed in the triaxial tests.

Analyses were carried out in terms of effective stresses modelling the clay layers as undrained and the other soils as drained.

Table 1. Soil properties.

Soil	γ (kN/m^3)	c' (kPa)	φ' (°)	OCR	K_0	E^{ref} (MPa)	m
MG	18.5	15	29	2.0	0.52	280	0.6
Silt	19.0	24	26	2.4	0.83	220	0.7
Sand	19.0	–	31	5	0.49	270	0.5
nc clay	18.6	24	25	1.1	0.60	120	0.9
Gravel	19.0	–	35	5	0.43	2100	0.5
oc clay	20.0	30	28	2.5	0.82	450	0.8

2.2 *Excavation model and structural properties*

The excavation consists of an elongated box with a length (66.8 m) to width (33.6 m) ratio of about 2 and a depth of about 40 m. Dimensions of the box excavation are typical of planned metro stations in the historical centre of Rome. The excavation is retained by diaphragm walls and by horizontal propping levels installed during the top down excavation sequence.

In the analyses the excavation was carried out in twelve stages, with seven levels of props constructed as excavation progresses. The wall behaves as an embedded cantilever up to the excavation level at +7.9 m o.d. (8.9 m depth), at which the first propping level is installed. The sequence of excavation and propping then continues to the final excavation level at –23 m o.d. (40 m depth). Figure 2 depicts schematically the final stages of excavation; 6 to 6.4 m of soil were excavated after the construction of each propping level constituted by the floor slabs, with the exception of temporary steel props installed at stage 9 at an elevation of –16.6 m o.d..

The perimeter retaining walls reach the deep layer of stiff clay, to prevent from uplift the excavation

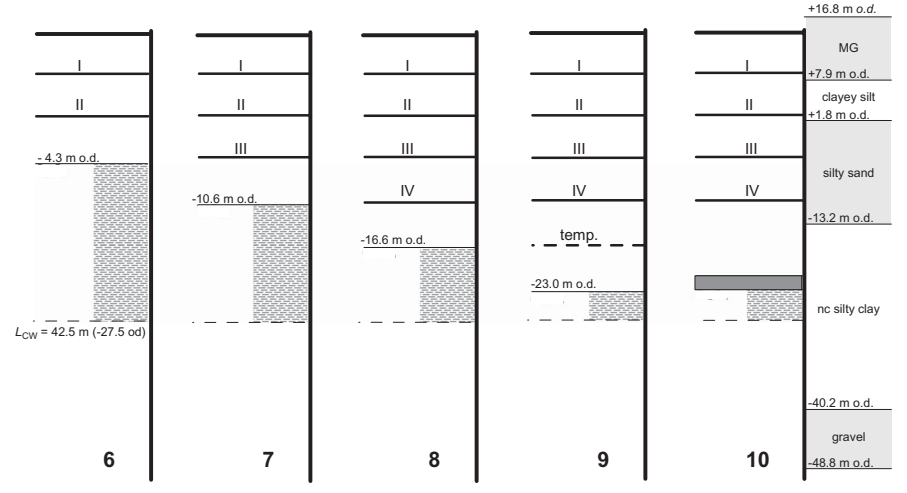

Figure 2. Excavation stages; cross-wall length $L_{cw} = 42.5$ m.

bottom and to minimise water flow within the excavation; they are assumed to be formed from reinforced concrete for a length of 55 m and from unreinforced concrete for the final portion, 10 m long.

Diaphragm wall panels, as well as cross-wall panels, were assumed to be 1.5 m thick and 2.8 m wide. Three lengths were considered for the sacrificial cross-walls: L_{cw} = 38 m that is equal to the maximum depth of excavation (–23 m o.d.); L_{cw} = 42.5 m and 47.0 m, for which the cross-wall toe is installed 4.5 and 9.0 m below the final excavation level (–27.5 m o.d. and –32.0 m o.d.), respectively.

Three values of cross-wall spacing were also assumed in the analyses (Fig. 3): s = 8.4, 11.2 and 22.4 m, with two, three and seven panels of diaphragm walls included in between the cross-walls. The ratio between the area occupied by the cross-walls and that of the soil within the excavation was A_{cw}/A_{soil} = 21.7, 15,4 and 7.2%, in the three cases.

Using symmetry, a portion of the box was considered in the analyses extending between the centre line of adjacent cross-walls as shown in the plan view of Figure 4 for a cross-wall spacing s = 8.4 m, so that a current central portion of the box excavation was modelled.

The 3D finite element mesh extends to about 100 m behind the diaphragm walls, that is 2.5 times the excavation depth, and up to the excavation centre line in front of it. Its height is about 2 times the final excavation depth (76.8 m). A 3D view of the domain analysed for cross-wall spacing s = 11.2 m is shown in Figure 5, without the soil inside the excavation.

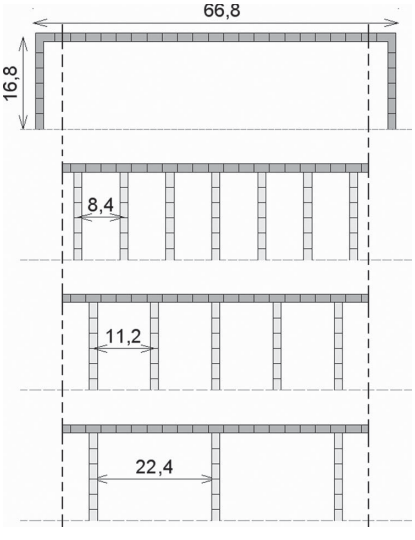

Figure 3. Analysed schemes of cross-walls systems.

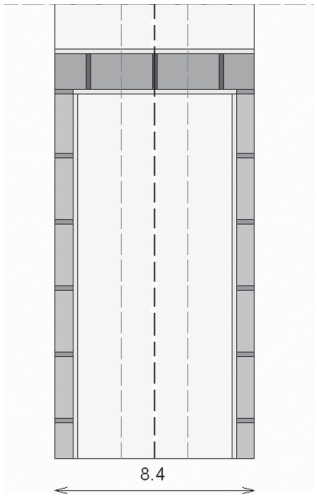

Figure 4. Plan view of the analysed domain for cross-wall spacing s = 8.4 m.

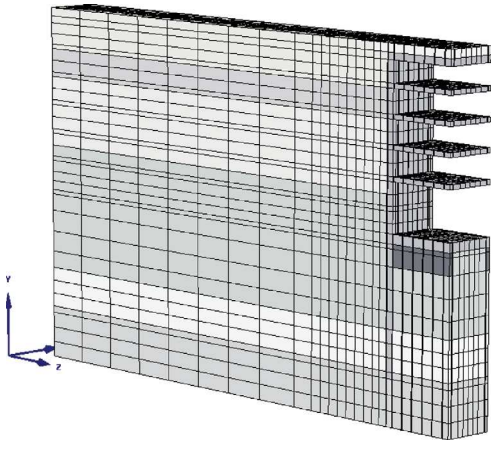

Figure 5. 3D view of the analysed domain for cross-wall spacing s = 11.2 m.

Both soil and structural elements were discretised with 15-noded linear strain wedges; 10240, 14144 and 37056 elements were used for the three values of cross-wall spacing.

All the structural elements were modelled as linear elastic materials with a Poisson coefficient $\nu' = 0.15$. The unit weight was $\gamma = 24$ and 25 kN/m^3 for unreinforced and reinforced concrete.

Cross-wall panels were assumed to be formed from unreinforced concrete of strength (and stiffness) lower than that of perimeter diaphragm walls; specifically, the cross-walls Young's modulus was 60% of that of diaphragm walls, $E_{cw} = 0.6\ E_{dw}$.

Stiffness of the floors of the box construction, acting as propping levels, was reduced to account for the presence of the lift and stair openings, also used to extract the soil during excavation; openings area was assumed to be 40% of the floor area in total.

Floor slabs were connected to the diaphragm walls through linear elastic interface elements, 0.2 m thick, with a stiffness reduced by about an order of magnitude to minimise the transmission of bending moment to the retaining wall ($E = 1.8$ GPa).

Table 2 summarises the properties of structural elements.

The temporary steel props installed at the elevation of −16.6 m o.d. were also modelled using brick elements, assuming a Young's modulus of 3 GPa to represent tubular steel props.

Soil–structure interfaces were modelled using finite elements 0.2 m thick (Fig. 4). The same constitutive model adopted for the soils was used, but with reduced strength and stiffness parameters (Table 3). Specifically, a reduction factor R_{int} was used for c' and tan φ', while the reduction was equal to R_{int}^2 for the Young's modulus.

Stiffness profile of soil–structure interfaces, and the stiffness decay with shear strain were described using the same values of m, E^{ref}/E^{ref}_{50}, $E^{ref}_{50}/E^{ref}_{oed}$ and ψ adopted for the soils.

The contacts between diaphragm wall panels and cross-wall panels, as well as the contacts between cross-walls and diaphragm walls were also modelled through finite elements, 0.2 m thick. The mechanical behaviour of these elements was described using a linear elastic—perfectly plastic Mohr—Coulomb model. The shear strength between the panels was characterised by negligible coesion, $c = 2$ kPa, a friction angle $\varphi = 35°$ and a dilatancy angle at failure $\psi = 10°$, while the stiffness was equal to that of the corresponding panels: $E = 36$ GPa for contacts between panels of diaphragm walls and $E = 22$ GPa for contacts between panels of cross-walls and between diaphragm walls and cross-walls.

Table 2. Stiffness of structural elements.

	f_{ck} (MPa)	Reduction	E' (GPa)
Reinforced perimeter wall	32	–	36.0
Unreinforced perimeter wall	12	–	22.0
Cross wall	12	–	22.0
Floor propping level	32	0.6	21.6
Bottom slab	32	–	36

Table 3. Soil–structure interface properties.

Soil	R_{int}	c'_{int} (kPa)	φ'_{int} (°)	E^{ref}_{int} (MPa)
Made ground	0.7	10.5	20	137
Clayey silt	0.7	16.8	18	108
Silty sand	0.7	–	22	132
nc silty clay	0.7	16.8	18	59
Gravel	1.0	–	35	210
oc silty clay	0.8	24	22	288

3 ANALYSIS RESULTS

3.1 *Three-dimensional finite element analyses*

Refinement of 3D meshes was evaluated through preliminary analyses carried under plane strain conditions (without cross-walls) using the 2D and the 3D suites of the code Plaxis. Soil and structural elements were discretised with 15-noded 3rd order strain triangles in the 2D model and with 15-noded linear strain wedges in the 3D model. Refinement of 3D meshes was assumed satisfying when differences of computed wall deflections were lower than 5% for all stages of excavation.

The results of 3D finite element analyses were examined to evaluate the effects of cross-walls spacing and length on the horizontal deflections of the perimeter diaphragm walls and the ground settlements behind the excavation. Both of them are in the following referred to the middle section between the cross-walls (dashed line in Fig. 4).

Figure 6 compares profiles of horizontal wall deflections computed for excavation to 40 m depth (stage 9), without cross-walls and with cross-walls of varying length, installed at different spacing. Table 4 summarises the computed values of maximum wall deflections.

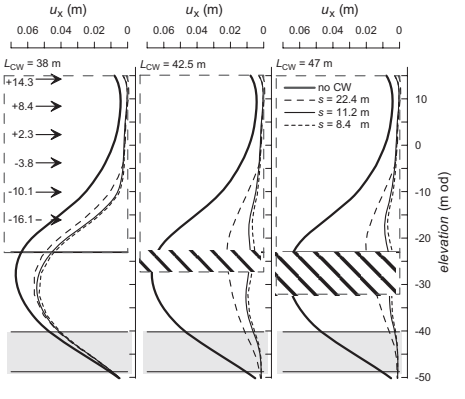

Figure 6. Effects of cross-walls spacing and length on wall deflections.

Table 4. Maximum wall deflections.

	No CW	s = 8.4 m	s = 11.2 m	s = 22.4 m
L_{cw} m	u_x mm	u_x mm	u_x mm	u_x mm
38.0	67.2	53.2	54.3	56.0
42.5		9.5	10.7	22.1
47.0		7.2	8.9	20.3

In all cases, the horizontal wall displacements are strongly reduced throughout the excavation depth, while a different behaviour is observed below the bottom of excavation depending on cross-walls length. For values of L_{cw} = 38 m, equal to the maximum excavated depth, a slight influence of cross-walls spacing is observed on the displacement profiles and the maximum wall deflection is about 20% lower than that computed without cross-walls. When cross-walls are prolonged below the final excavation level, horizontal deflections strongly reduce also below the formation level and the influence of cross-walls spacing becomes more evident. For a cross-walls length L_{cw} = 42.5 m (4.5 m depth below the excavation bottom) the maximum wall deflection reduces of about 85% using a cross-wall spacing s = 8.4–11.2 m and of about 67% using s = 22.4 m. A further increase in cross-walls length, L_{cw} = 47 m, (9.0 m depth below the excavation bottom) provides a further reduction of maximum wall displacement (≅ 90% for s = 8.4–1.2 m and 70% for s = 22.4 m), although the benefit of increasing L_{cw} reduces for higher cross-walls spacings. Limited extension of cross-walls length below the final excavation level then produces a significant reduction of wall deflections along the embedded portion of the retaining walls.

Figure 7 shows variation of horizontal deflections along the diaphragm wall at –19 m o.d., 3 m below the temporary propping level and at the excavation level (–23 m o.d.) for the case of L_{cw} = 42.5 m. Wall displacements smoothly increase with distance from cross-walls with negligible relative displacements between the panels of the diaphragm walls.

Sufficient connection between wall panels was then provided by the strength properties assumed for the interface elements and by the contribution of both the temporary props and the soil below the excavation level. Similar trends were computed from additional analyses in which the friction and the dilatancy angles were reduced to 30° and 5°, respectively.

Figure 8 shows the displacement field computed without cross-walls and with cross-walls of different length installed at spacing s = 11.2 m; the

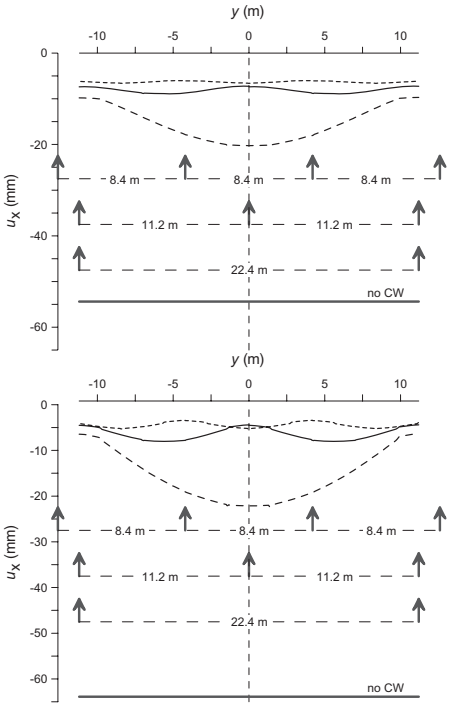

Figure 7. Maximum horizontal deflections of perimeter diaphragm walls with varying cross-wall spacing: a) –19 m o.d; b) –23 m o.d.

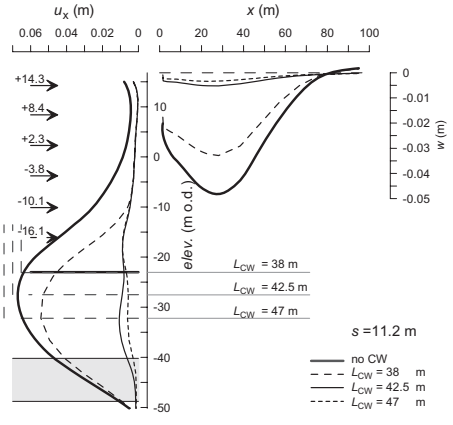

Figure 8. Effect of cross-wall length on displacement field at constant cross-wall spacing s = 11.2 m.

results refer to the final excavation level at –23 m o.d. (40 m depth). Both wall deflections and ground surface settlement profile behind the excavation are for the mid-section in between the cross-walls. Table 5 reports the maximum surface

Table 5. Maximum surface settlements.

	No CW	L_{cw} = 38.0 m	L_{cw} = 42.5 m	L_{cw} = 47.0 m
w_{max} (mm)	48.2	32.9	5.2	3.4

settlements, obtained at a distance of about 30 m from the wall.

Consistently with reduction of wall deflections, cross-walls also reduce substantially the magnitude of surface settlements. Specifically, benefit increases with cross-walls length, settlement reduction varying from about 32% for L_{cw} = 38 m to about 90% for L_{cw} = 42.5–47 m. Surface settlements also reduce with decreasing cross-walls spacing although limited benefit is obtained for $s < 11.2$ m.

3.2 *Plane strain finite element analyses*

To evaluate the capability of predicting the performance of deep excavations with sacrificial cross-walls assuming plane strain conditions, comparison 2D finite element analyses were finally carried out.

In the analyses, the soil and the cross-walls within the excavation were modelled as an equivalent homogenous material with linear elastic behaviour, while the interface between the equivalent material and the diaphragm walls was described using a linear elastic—perfectly plastic Mohr—Coulomb model.

Properties of the equivalent homogeneous material were obtained averaging the soil and the cross-walls properties, weighted on the corresponding dimensions occupied in plan. The equivalent Young's modulus was for example evaluated using the relationship:

$$E_{eq} = \frac{E_{cw} \cdot t + E_s \cdot (s - t)}{s} \quad (2)$$

where t and s are the cross-walls thickness and spacing and E_{cw} and E_s are the cross-walls and soil Young's moduli.

Preliminarily to this, average soil properties were evaluated for the soil layers included throughout the cross-walls length, considering the layers thickness as a weighting factor. Due to the assumed linear elastic behaviour, soil stiffness was computed using the values of E'_{50} at the mid point of each layer, that can be thought to be representative of stiffness at average strain levels, rather than using the values of E' that were linked to the small-strain shear modulus G_0. Similar values of average soil properties were obtained for the different cross-walls lengths, so that the following quantities were assumed: $\gamma = 18.8$ kN/m^3, $E' = 22$ MPa, $c' = 14$ kPa and $\varphi' = 28°$.

The unit weight and the stiffness of equivalent material were slightly affected by cross-walls length as well, so that a single value of γ_{eq} and E_{eq}' were assumed for each cross-walls spacing (Table 6).

Strength parameters of interfaces elements between the equivalent material and the diaphragm walls were obtained using relationships similar to Eq. (2) for c_{eq} and tan φ_{eq} and a reduction factor $R_{int} = 0.7$. Again, similar values were obtained irrespective of cross-walls length and spacing thus assuming $c_{int} = 9$ kPa and $\varphi_{int} = 21°$. Stiffness of interface elements was instead obtained multiplying the values of E_{eq} in Table 6 for the reduction factor $R_{int}^2 = 0.49$.

Figure 9 compares profiles of wall deflections computed for stage 9, when the final excavation level is reached, under 2D and 3D conditions; results refer to cross-walls length L_{cw} = 42.5 m (–27.5 m o.d.).

For values of $s = 8.4$ and 11.2 m, the plane strain analyses, in which the cross-walls and the soil within the excavation are described by an equivalent material, provide a fair estimate of wall deflections along the excavated depth, while horizontal wall displacements are overestimated below the final excavation levels, when assuming plane strain conditions.

Specifically, maximum wall displacements computed in the 2D analyses are of about 2 times greater than those computed in the 3D analyses and occur at higher depths. Significant differences in the deflection profiles are instead observed for $s = 22.4$ m, for which the three-dimensional pattern of behaviour is more relevant.

Similarly to the results obtained for the wall deflections, plane strain analyses also provide an overestimate of ground surface settlement profiles behind the wall, as shown in Figure 10 for L_{cw} = 42.5 m; again, for s = 8.4 and 11.2 m maximum settlements computed under 2D conditions are about 2 times greater than the ones computed under 3D conditions.

Then, plane strain analyses in which an equivalent material was used to represent the soil and the cross-walls within the excavation provided an overestimate of wall deflections and ground movements. However, significant differences in

Table 6. Young's moduli of the equivalent material.

	s = 8.4 m	s = 11.2 m	s = 22.4 m
E_{eq}'(MPa)	3950	2965	1494
γ_{eq} (kN/m^3)	19.7	19.5	19.1

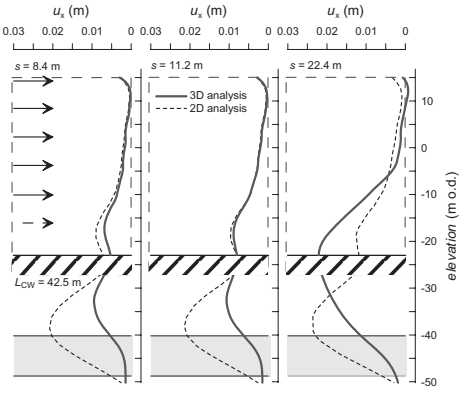

Figure 9. Horizontal displacement of the diaphragm walls computed by 3D and 2D finite element analyses.

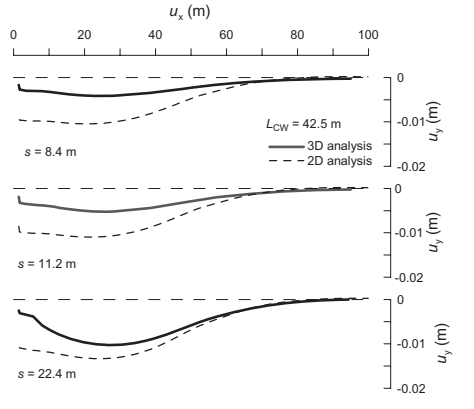

Figure 10. Surface settlement profiles computed by 3D and 2D analyses: L_{cw} = 42.5 m, s = 11.2 m.

profiles of wall deflections were obtained from 2D and 3D analyses when cross-walls spacing was increased to s = 22.4, due to the increasing influence of the 3D displacement field.

4 CONCLUSIONS

3D finite element analyses of deep excavations with sacrificial cross-walls were carried out to assess the effectiveness of cross-walls as a mitigation measure for reducing the horizontal deflections of diaphragm walls and the ground settlements around the excavation. In the analyses, a portion of the box excavation was modelled extending between the centre line of two adjacent cross-walls. Both soil and structural elements, including the cross-walls, were described by 15-noded linear strain wedges, using interface elements to model the soil–structure contacts and the contacts between the structural elements, such as those between the panels of diaphragm walls and of cross-walls.

Specifically, the analyses were performed to investigate the effects of cross-walls length and spacing on the ground movements induced by the excavation, considering a soil profile typical of central Rome.

The results show that sacrificial cross-walls permit to reduce substantially the diaphragm wall deflections and the ground surface settlements behind the perimeter diaphragm walls. Ground movement reduces further prolonging the cross-walls below the final excavation depth and reducing cross-wall spacing. However, a reducing benefit was observed for values of cross-walls embedded length greater than 4.5 m and for cross-walls spacing lower than 11.2 m.

Comparison 2D analyses were also carried out to evaluate the capability of predicting the performance of a deep excavation in which cross-walls are used as a mitigation measure to reduce ground movements. In the analyses, an equivalent material was modelled to represent the cross-walls and the soil within the excavation. For cross-wall spacing s = 8.4 and 11.2 m., a fair agreement was obtained for wall displacements computed throughout the excavated depth, while an overestimate was obtained for wall deflections computed below the excavation bottom and for the ground surface settlement profiles behind the excavation. On the other side, profiles of wall deflections computed by 2D and 3D analyses differed substantially for s = 22.4 m, for which the 3D patterns of behaviour strongly affect the computed displacement field.

ACKNOWLEDGEMENTS

The Authors wish to thank Mrs F. Buono and Dr G. Landi for useful information on soil data and Prof. L. Callisto for fruitful discussions and suggestions.

REFERENCES

Bailey R.P., Harris D.I. and Jenkings M.M. (1999). Design and construction of Westminster station on the Jubilee Line Extension. *Proc. Instn Civ. Engrs Civ. Engng Jubilee Line Extension*, 132: 36–46.

Burland J.B., Simpson B. and St John H.D. (1979). Movements around excavations in London Clay. *Proc. 7th ECSMFE*, Brighton, 1: 13–29.

Hsieh H.S., Lu Y.C. and Lin T.M. (2008) Effects of joint details on the behaviour of cross walls. *Journal of Geo Engineering*, 3 (2): 55–60.

Hsiung B.C.B., Nash D.F.T., Cheng K.H., Huang C.C. and Hwang, R.N.H. (2001). The effectiveness of jet-grout slabs and cross-walls in restricting wall movements in deep excavations. *Proc. 14th Southeast Asia Geotech. Engng Conference*, Hong Kong, China.

Merritt A.S., Menkiti C.O., Harris D.I., Zdravkovic L., Potts D.M. and Mair R.J. (2010). 3D finite element analysis of a diaphragm wall excavation with sacrificial crosswalls. *In Geotechnical Challenges in Megacities, GeoMos2010, Int. Geotech. Conf.*, Moscow, Russia.

Osborne N.H., Ng C.C. and Cheah C.K. (2009). The benefits of hybrid ground treatment in significantly reducing wall movements: A Singapore case history. *In Geotechnical aspects of underground construction in soft ground*. Ng, Huang & Liu (eds), Taylor & Francis Group, London, 447–453.

Ou C.Y., Hsieh P.G. and Lin Y.L. (2011) Performance of excavation with cross walls. *Journal of Geotechnical and Geoenvironmental Engineering*, ASCE, 137 (1), 94–104.

Ou C.Y., Lin Y.L. and Hsieh P.G. (2006). Case records of an excavation with cross walls and buttress walls. *Journal of Geo Engineering*, 1 (2): 79–86.

Schanz, T., Vermeer, P., Bonnier, P. 1999. Formulation and Verification of the Hardening-Soil Model. *Proc. Plaxis Symposium Beyond 2000 in Computational Geotechnics*, Amsterdam, the Netherlands, 281–296.

Stevens A., Corbett B.O. and Steele A.J. (1977). Barbican Arts Centre: the design and construction of the substructure. *The Structural Engineer*, 55 (11): 473–485.